

# Paclitaxel delivery from cobalt-chromium alloy surfaces using self-assembled monolayers

Gopinath Mani<sup>a)</sup>

Biomedical Engineering Program, University of South Dakota, Sioux Falls, South Dakota 57107

Nelson Torres and Sunho Oh

Department of Biomedical Engineering, University of Texas at San Antonio, San Antonio, Texas 78249

(Received 26 January 2011; accepted 21 March 2011; published 8 April 2011)

Polymer-based platforms in drug-eluting stents (DESs) can cause adverse reactions in patients. Hence, the development of a polymer-free drug delivery platform may reduce adverse reactions to DES. In this study, the use of a polymer-free platform, self-assembled monolayers (SAMs), is explored for delivering an antiproliferative drug [paclitaxel (PAT)] from a stent material [cobalt-chromium ((Co—Cr) alloy)]. Initially, carboxylic acid terminated phosphonic acid SAMs were coated on Co—Cr alloy. Two different doses (25 and 100  $\mu\text{g}/\text{cm}^2$ ) of PAT were coated on SAM coated Co—Cr surfaces using a microdrop deposition method. Also, control experiments were carried out to coat PAT directly on Co—Cr surfaces with no SAM modification. The PAT coated specimens were characterized using the Fourier transform infrared spectroscopy (FTIR), scanning electron microscopy (SEM), and atomic force microscopy (AFM). FTIR spectra showed the successful deposition of PAT on SAM coated and control-Co—Cr surfaces. SEM images showed islands of high density PAT crystals on SAM coated surfaces, while low density PAT crystals were observed on control-Co—Cr alloy. AFM images showed molecular distribution of PAT on SAM coated as well as control-Co—Cr alloy surfaces. *In vitro* drug release studies showed that PAT was released from SAM coated Co—Cr surfaces in a biphasic manner (an initial burst release in first 7 days was followed by a slow release for up to 35 days), while the PAT was burst released from control-Co—Cr surfaces within 1–3 days. Thus, this study demonstrated the use of SAMs for delivering PAT from Co—Cr alloy surfaces for potential use in drug-eluting stents.

© 2011 American Vacuum Society. [DOI: 10.1116/1.3575530]

## I. INTRODUCTION

Coronary artery disease (CAD) is one of the leading causes of death for both men and women throughout the world.<sup>1</sup> CAD occurs mainly due to the deposition of plaque in the blood vessels which supply oxygen-rich blood to the heart.<sup>1</sup> Balloon angioplasty is the technique that has been commonly used to treat CAD.<sup>2,3</sup> However, restenosis (renarrowing of arteries) occurs in 30%–40% of the patients within 6 months after angioplasty treatment.<sup>4,5</sup> To overcome this limitation, coronary stents are implanted following balloon angioplasty to help keeping the artery open.<sup>4,5</sup> However, endothelial cell damage occurs during stent implantation and it causes a whole cascade of events resulting in neointimal hyperplasia (NH).<sup>6</sup> NH is characterized by the migration and proliferation of smooth muscle cells followed by extracellular matrix synthesis and deposition.<sup>7</sup> NH is primarily responsible for in-stent restenosis (renarrowing of the arteries after stent implantation).<sup>8</sup> Drug-eluting stents (DESs) are currently implanted to treat in-stent restenosis.<sup>9</sup> Stents are coated with an antiproliferative drug and the drug is released for a period of time to control the growth the smooth muscle cells.<sup>9</sup> Although the implantation of DES significantly reduced the incidences of in-stent restenosis, some drawbacks are still associated with its use.<sup>10</sup> Most commercially available DESs

use polymers to coat and release drugs. The limitations of using some polymeric carriers in DES are as follows: (a) polymer coatings undergo cracks, fissures, waviness, and other irregularities during stent expansion;<sup>11</sup> (b) inflammatory and hypersensitivity reactions to polymer coatings;<sup>12–18</sup> and (c) polymer coatings affect the normal vessel healing process<sup>17,19,20</sup> and this could cause late stent thrombosis.<sup>18,19,21</sup> Hence, there is a need for developing polymer-free drug delivery platform for coronary stents.

Recently, we successfully demonstrated the use of self-assembled monolayers (SAMs) as a polymer-free drug delivery platform for stents with no adverse response from endothelial cells.<sup>22,23</sup> However, some technical challenges remained in the use of SAMs as an effective drug delivery platform for stents. The objectives of this study are to overcome the technical challenges listed below. First, our previous studies were carried out using model substrates (gold and titanium) and a model drug (flufenamic acid).<sup>22</sup> Hence, the first objective of this study is to adapt SAM based platform to release an antiproliferative drug [paclitaxel (PAT)] from a stent material [cobalt-chromium (Co—Cr) alloy]. Second, the amount of drug that was coated using SAMs was in  $\text{ng}/\text{cm}^2$ .<sup>22</sup> Hence, the second objective of this study is to increase the amount of drug coated using SAM platform to levels comparable to those employed in currently available DES (in  $\mu\text{g}/\text{cm}^2$ ).

<sup>a)</sup>Electronic mail: gopinath.mani@usd.edu

## II. EXPERIMENT

### A. Materials

Ethanol (200 proof) was purchased from Pharmco-AAPER (USA). Acetone, methanol, 16-phosphonohexadecanoic acid (16-PHDA), and phosphate buffered saline with 0.05% tween-20 (PBS/T-20) were all purchased from Sigma-Aldrich (USA). Anhydrous tetrahydrofuran (THF) was purchased from Alfa-Aesar (USA). PAT was purchased from ChemieTek (Indianapolis, IN). All chemicals were used as received. Co—Cr alloy (L605) was purchased from High Temp Metals, Inc. (Sylmar, CA).

### B. Preparation of control-Co—Cr alloy

Co—Cr alloy samples (length  $\times$  width  $\times$  thickness = 1 cm  $\times$  1 cm  $\times$  1 mm) were chemically cleaned by sonication in ethanol, acetone, and methanol twice for 10 min each. The samples were then dried under nitrogen ( $N_2$ ) gas. Thus, prepared chemically cleaned Co—Cr alloy samples are referred to here as control-Co—Cr (Ctrl-Co—Cr).

### C. Coating of SAMs on Co—Cr alloy

The chemically cleaned Co—Cr alloy samples were immersed in 1 mM solution of 16-PHDA in THF for 18 h. The samples were taken out of the THF solution and transferred to an oven without rinsing. In the oven, the samples were heated in air at 120 °C for 18 h. The samples were then sonicated in THF and double-distilled water (dd- $H_2O$ ) for 1 min each followed by  $N_2$  gas drying. Thus, prepared SAM coated Co—Cr alloy samples are referred to here as SAM-Co—Cr.

### D. Coating of PAT on control and SAM coated Co—Cr alloy

PAT was coated on control and SAM coated surfaces by a microdrop deposition method as reported previously with slight modification.<sup>24</sup> Briefly, PAT solutions were prepared in ethanol at two different concentrations of 0.5 and 2 mg/ml. Two different drug doses of 25 and 100  $\mu\text{g}/\text{cm}^2$  were prepared by dropping a 50  $\mu\text{l}$  aliquot of the prepared PAT solutions of concentrations of 0.5 and 2 mg/ml, respectively, on control and SAM coated alloy surfaces (1  $\times$  1  $\text{cm}^2$ ). The ethanol was allowed to evaporate under ambient laboratory conditions for 3 h leaving behind a residue of PAT on the alloy specimens. All PAT coated specimens were then transferred to an oven and heated in air at 140 °C for 3 h.

A schematic of the preparation of PAT coated samples is shown in Fig. 1. Control-Co—Cr alloy samples with PAT loadings of 25 and 100  $\mu\text{g}/\text{cm}^2$  are referred to here as Ctrl-PAT-25 and Ctrl-PAT-100, respectively. SAM coated Co—Cr alloy samples with drug loadings of 25 and 100  $\mu\text{g}/\text{cm}^2$  are referred to here as SAM-PAT-25 and SAM-PAT-100, respectively. A list of abbreviations used in the article and their descriptions is provided in Table I.

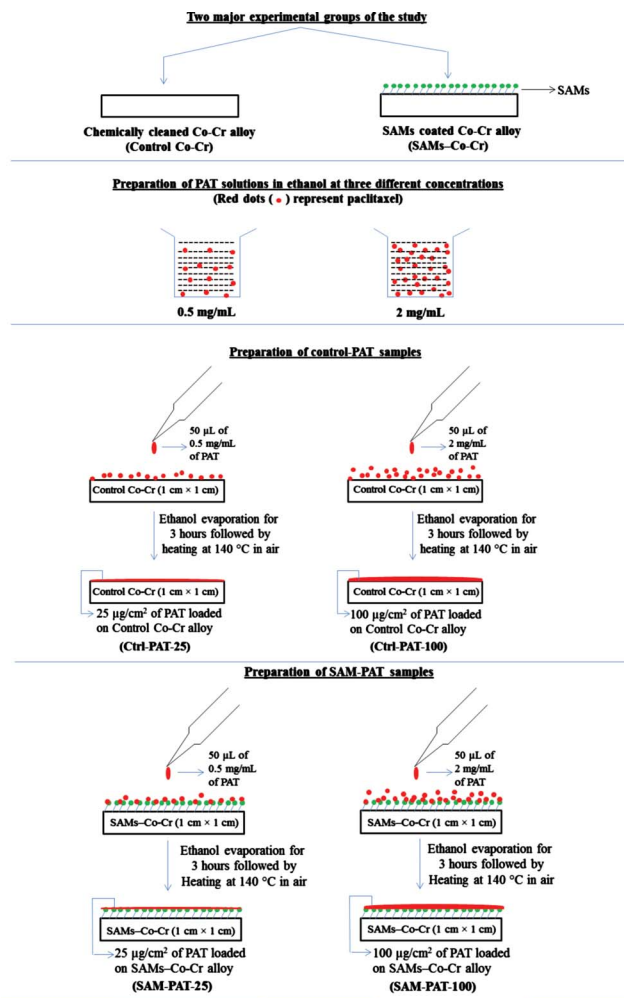


Fig. 1. (Color online) Schematic of the preparation of PAT deposited control and SAM coated Co—Cr alloy samples.

### E. Surface characterization

The control, SAM coated, and PAT coated Co—Cr alloy specimens were characterized using Fourier transform infrared spectroscopy (FTIR), scanning electron microscopy (SEM), and atomic force microscopy (AFM). X-ray photoelectron spectroscopy (XPS) was also used to characterize control and SAM coated specimens.

TABLE I. List of abbreviations used in the study and their descriptions.

Abbreviations used	Descriptions
Co—Cr alloy	Cobalt-chromium alloy
Ctrl-Co—Cr	Chemically cleaned cobalt-chromium alloy
SAM-Co—Cr	SAM coated Co—Cr alloy
Ctrl-PAT	PAT deposited control-Co—Cr alloy
Ctrl-PAT-25	25 $\mu\text{g}/\text{cm}^2$ of PAT deposited control-Co—Cr alloy
Ctrl-PAT-100	100 $\mu\text{g}/\text{cm}^2$ of PAT deposited control-Co—Cr alloy
SAM-PAT	PAT deposited SAM coated Co—Cr alloy
SAM-PAT-25	25 $\mu\text{g}/\text{cm}^2$ of PAT deposited SAM coated Co—Cr alloy
SAM-PAT-100	100 $\mu\text{g}/\text{cm}^2$ of PAT deposited SAM coated Co—Cr alloy

## 1. FTIR

A Nicolet 6700 FTIR instrument (Thermo Scientific) equipped with an attenuated total reflection accessory was used in this study. The number of scans used to collect each infrared spectrum was 32 and a spectral resolution of  $4\text{ cm}^{-1}$  was used. All the IR spectra reported in this study were baseline corrected using OMNIC software.

## 2. SEM

A EVO-40SEM from ZEISS (Germany) was used in this study. An accelerating voltage of 10.00 kV was used at a working distance of 30–32 mm. The specimens were sputter coated with a 5 nm thin layer of carbon or gold-palladium prior to SEM imaging.

## 3. AFM

A Nanoscope III multimode AFM from Digital Instruments, Inc. (Santa Barbara, CA) was used in this study. All images were captured using tapping mode at a scan size of  $10 \times 10\ \mu\text{m}^2$ . Silicon nitride cantilevers with a spring constant of 20 N/m were used to scan the specimens. The imaging was carried out in air at room temperature. All captured images were subjected to flattening according to third degree polynomial fit. The rms roughness values represent the mean  $\pm$  standard deviation of data collected from three different spots ( $10 \times 10\ \mu\text{m}^2$ ) of a specimen.

## 4. XPS

XPS measurements were carried out using a Kratos Axis Ultra instrument equipped with a monochromatized Al  $K\alpha$  x-ray source ( $E=1486.7\text{ eV}$ , 227 W), a hemispherical energy analyzer, and a channeltron detector array. A photoelectron takeoff angle of  $90^\circ$  from the surface was used in this study. Survey scans were obtained using a pass energy of 160 eV and high resolution scans were obtained using pass energies of 20 eV for C 1s and O 1s spectra and 40 eV for all the other elements (Co 2p, Cr 2p, W 4f, Ni 2p, P 2p, and N 1s) analyzed in this study. Data calibration for all the obtained spectra was carried out by setting the C 1s hydrocarbon peak at 285 eV. CASA XPS software was used to deconvolute the spectra, to analyze the peak areas, and to calculate the atomic percentage concentrations of elements and molar percentage concentrations of components.

## F. Drug-elution studies

PAT coated control ( $n=4$ ) and SAM coated ( $n=4$ ) alloy samples were immersed in 2 ml of PBS/T-20 solution (PBS containing 0.05% Tween-20,  $\text{pH}=7.4$ ) and placed in a water bath at  $37^\circ\text{C}$  for up to 35 days. Tween-20, a nonionic surfactant, was added to the PBS to increase the solubility of PAT and to maintain sink conditions.<sup>25–28</sup> At predetermined time points (1, 3, 5, 7, 14, 21, 28, and 35 days), the alloy samples were taken out of the incubated PBS/T-20 solution and immediately transferred to fresh PBS/T-20 solution for the next time point. The PBS/T-20 solutions collected at each time point were then used to calculate the amount of drug

released using high performance liquid chromatography (HPLC). As previously described,<sup>24</sup> 1 ml of ethanol was added to the polypropylene tubes in which the PBS/T-20 solutions were collected. This step was carried out before analyzing the collected solutions using HPLC. Ethanol addition was carried out to remove any PAT molecules physically adsorbed on the polypropylene tube surfaces and to improve the solubility of PAT in PBS/T-20.<sup>24,29,30</sup> This would improve the accuracy of quantifying the released PAT using HPLC.

## 1. High performance liquid chromatography

HPLC analysis was carried out using a Waters Alliance System which included a Waters e2695 separations module, a Waters 2489 UV/visible detector, and a reverse-phase Waters Nova-Pak C18  $4\ \mu\text{m}$  column. The separations were carried out using a mobile phase composition of 45% water and 55% acetonitrile at a flow rate of 1 ml/min. The column temperature was maintained at  $35^\circ\text{C}$  during the separation. A sample volume of  $10\ \mu\text{l}$  was used for the analysis. UV detection was carried out at a wavelength of 227 nm. Calibration standards were prepared from the solution of PAT in ethanol. PAT solutions at concentrations ranging from 100  $\mu\text{g/ml}$  to 1 ng/ml in ethanol were prepared. Calibration graphs of PAT were obtained by plotting the area of the peak ( $\mu\text{V/s}$ ) in  $y$ -axis and concentrations of the drug ( $\mu\text{g/ml}$  or ng/ml) in  $x$ -axis. The graphs were linear over the concentration ranges of 100  $\mu\text{g/ml}$ –99 ng/ml and 99–1 ng/ml with correlation coefficients of  $R^2$  values of 0.9922 and 0.9969, respectively. All HPLC data were analyzed using a WATERS EMPower 2 software system.

## G. Statistical analysis

The experimental data collected in this study are presented as mean  $\pm$  standard deviation. A one-way analysis of variance (ANOVA) was used to determine the statistical significant differences at  $p < 0.05$ .

## III. RESULTS

### A. Surface characterization of Ctrl-Co—Cr and SAM-Co—Cr before and after PAT coating

XPS and FTIR were used to characterize the SAM coating on Co—Cr alloy. PAT deposited alloy specimens (Ctrl-PAT series and SAM-PAT series) were characterized using FTIR, SEM, and AFM for studying the coating, morphology, and distribution of PAT on alloy surfaces.

#### 1. XPS characterization

High resolution XPS C 1s, O 1s, N 1s, Co 2p, Cr 2p, W 4f, Ni 2p, and P 2p spectra were collected for control and SAM coated specimens. The atomic percentage concentrations of all the elements scanned in this study were provided in (a) in Table II. No XPS peak for phosphorous was detected for Ctrl-Co—Cr alloy specimens. However, after the deposition of phosphonic acid SAM, the P 2p peak at  $133.6 \pm 0.3$  was observed. The atomic percentage concentration of P 2p for SAM coated Co—Cr alloy was  $2.9\% \pm 1\%$

TABLE II. XPS determined atomic percentage concentrations (a), molar percentage concentrations of C 1s (b) and O 1s (c) components of control, SAM coated, and PAT coated specimens.

(a)								
Samples	C 1s	O 1s	N 1s	Co 2p	Cr 2p	W 4f	Ni 2p	P 2p
Ctrl	48.5 ± 1.9	38.2 ± 1.4	1.0 ± 0.2	3.5 ± 0.3	6.8 ± 0.4	1.5 ± 0.1	0.9 ± 0.1	ND <sup>a</sup>
SAM coated	57.4 ± 8.3	32.9 ± 6.9	0.9 ± 0.4	1.1 ± 0.6	3.5 ± 1.5	1.0 ± 0.4	0.4 ± 0.2	2.9 ± 1.0

(b)						
Samples	C 1s (1)		C 1s (2)		C 1s (3)	
	BE (eV)	Molar percentage concentration of components	BE (eV)	Molar percentage concentration of components	BE (eV)	Molar percentage concentration of components
Ctrl	285	66.2 ± 2.5	286.4 ± 0.1	20.4 ± 2.0	288.8	13.4 ± 1
SAM coated	285	74.2 ± 2.5	286.2 ± 0.3	18.2 ± 2.1	289	7.6 ± 1.5

(c)						
Samples	O 1s (1)		O 1s (2)		O 1s (3)	
	BE (eV)	Molar percentage concentration of components	BE (eV)	Molar percentage concentration of components	BE (eV)	Molar percentage concentration of components
Ctrl	530	19.5 ± 1	531.6	74.6 ± 1.6	533.7 ± 0.1	5.9 ± 0.9
SAM coated	530.4 ± 0.4	17.5 ± 10.7	532.1 ± 0.3	71.5 ± 8.2	533.7 ± 0.3	11.0 ± 7.4

<sup>a</sup>ND=Not detected.

[(a) in Table II]. Also, a significant increase in the concentration of carbon was accompanied by a significant decrease in the concentrations of oxygen, cobalt, chromium, tungsten, and nickel atoms after the deposition of SAM [(a) in Table II]. Since the SAM is primarily composed of carbon atoms, the concentration of carbon is expected to increase after the deposition of monolayer. Also, the concentrations of oxygen (the primary element in the surface oxide layer of Co—Cr) and other elements (Co, Cr, W, and Ni) in the alloy substrate are expected to decrease due to the attenuation of XPS signals. The C 1s spectrum of Ctrl-Co—Cr alloy was deconvoluted into three components: the peaks at 285, 286.4 ± 0.1, and 288.8 eV were assigned to carbon atoms in C—C, C—OH, and C=O species of hydrocarbon contaminants [(b) in Table II]. Several studies have showed the presence of such hydrocarbon contaminant species on different metal oxides.<sup>31–34</sup> Also, the C—C peak of hydrocarbon contamination at 285 eV has been commonly used as an internal standard for XPS calibration.<sup>34</sup> The C 1s spectrum of SAM-Co—Cr alloy was deconvoluted into three components as well. The peaks at 285, 286.2 ± 0.3, and 289 eV were assigned to carbon atoms in C—C, C—O, and C=O species of SAM molecules [(b) in Table II]. The O 1s spectrum of Ctrl-Co—Cr alloy was deconvoluted into three components: the peaks at 530, 531.6, and 533.7 ± 0.1 eV were assigned to metal oxide (O<sub>2</sub><sup>−</sup>), metal hydroxide (OH<sup>−</sup>), and water (H<sub>2</sub>O) species, respectively [(c) in Table II]. After SAM coating, the peaks of O 1s components at 530.4 ± 0.4, 532.1 ± 0.3, and 533.7 ± 0.3 eV were assigned to oxygen atoms in metal oxide, P—O—metal/P=O, and P—OH/C—OH, respectively [(c) in Table II]. These results are in agreement with the literature on the formation of phosphonic acid SAMs on other metal oxides.<sup>35,36</sup>

## 2. FTIR characterization

The asymmetric ( $\nu_{\text{asym}}$ ) and symmetric ( $\nu_{\text{sym}}$ ) stretches of —CH<sub>2</sub> groups have been commonly used to study the ordering of monolayers on various substrates.<sup>33,37–40</sup> Typically, for a well-ordered monolayer, the peaks of  $\nu_{\text{asym}}(\text{CH}_2)$  and  $\nu_{\text{sym}}(\text{CH}_2)$  have been observed at <2918 and <2850 cm<sup>−1</sup>, respectively.<sup>33,37,38</sup> In our study, the peaks of  $\nu_{\text{asym}}(\text{CH}_2)$  and  $\nu_{\text{sym}}(\text{CH}_2)$  were observed at 2917 and 2849 cm<sup>−1</sup>, respectively [Fig. 2(a)]. These results suggested that the phosphonic acid molecules formed an ordered monolayer on Co—Cr alloy substrates. The peak observed for C=O stretching at 1705 cm<sup>−1</sup> shows the presence of —COOH terminal groups of SAMs. In the literature, the shift and broadening of peaks for P—O group stretches ( $\nu_{\text{P—O}}$ ) have been used to study the bonding of phosphonic acid molecules on variety of metal oxide substrates.<sup>39</sup> The peak for  $\nu_{\text{P—O}}$  of phosphonic acid molecules has been observed at 1075 cm<sup>−1</sup> before bonding to metal surfaces.<sup>39</sup> However, after the molecules were chemically bound to alloy surfaces, the peak was broadened and shifted to 1055 cm<sup>−1</sup>.<sup>39</sup> Consistent with the literature, in our study, the broad peak observed at 1062 cm<sup>−1</sup> shows the presence of P—O groups of phosphonic acid molecules chemically bound to Co—Cr alloy surfaces.

The FTIR spectrum of PAT in powder form was obtained [Fig. 2(b)]. The strong absorption bands for the C=O stretches of ester, ketone, and amide groups were observed at peaks of 1729, 1700, and 1639 cm<sup>−1</sup>, respectively. The peaks for the finger print regions of PAT were observed at 1242, 1072, and 707 cm<sup>−1</sup>. The peak positions of PAT observed in our study are in well agreement with the previously reported studies.<sup>41,42</sup> Figure 2(c) shows the infrared spectrum of PAT (in powder form) which was heated to 140 °C for 3

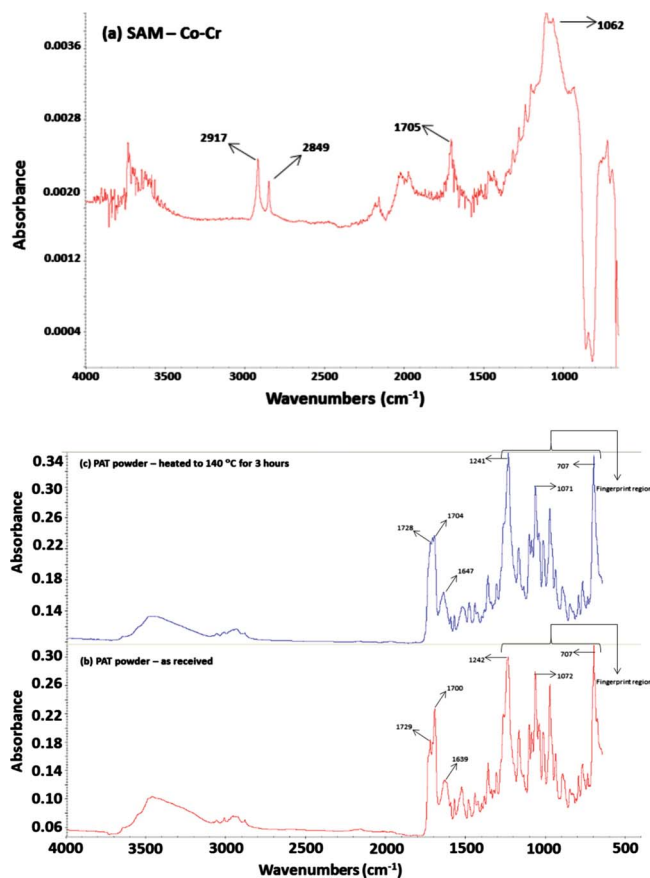


Fig. 2. (Color online) FTIR spectrum of SAM-Co—Cr (a), as-received PAT powder (b), and PAT powder heated to 140 °C for 3 h (c).

h. This experiment was conducted to verify that the temperature of 140 °C used in the drug attachment protocols would not make any changes in the chemical structure of PAT. Similar to as-received PAT [Fig. 2(b)], the strong absorption bands for the C=O stretches of ester, ketone, and amide groups and finger print regions were present in the IR spectrum of PAT heated to 140 °C [Fig. 2(c)]. These results demonstrated that the heat treatment involved in the drug attachment protocol did not induce any changes in the chemical structure of PAT. These results were also consistent with the literature on thermal stability of PAT.<sup>43</sup> Liggins *et al.*<sup>43</sup> investigated the thermal stability of PAT using differential scanning calorimetry (DSC) and thermogravimetric analysis (TGA). DSC showed no transitions of PAT before the drug reached its melting point at 220 °C. Also, TGA showed no weight loss of PAT until it reached its melting point. Hence, the temperature of 140 °C used in the drug attachment protocol would not affect the physiochemical properties of PAT.

Figures 3(a) and 3(b) show the FTIR spectra of Ctrl-PAT-25 and Ctrl-PAT-100, respectively. Figures 3(c) and 3(d) show the FTIR spectra of SAM-PAT-25 and SAM-PAT-100, respectively. The C=O stretches of ester, ketone, and amide groups and finger print regions of PAT were observed on all the specimens. Also, the intensity of the peaks increased depending on the amount of drug loaded on the alloy surfaces. This behavior was observed for both Ctrl-PAT and SAM-PAT

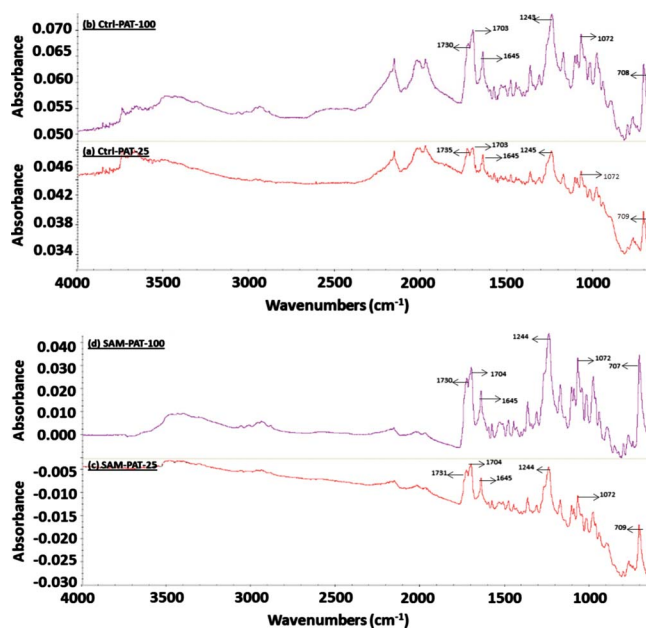


Fig. 3. (Color online) FTIR spectra of Ctrl-PAT-25 (a), Ctrl-PAT-100 (b), SAM-PAT-25 (c), and SAM-PAT-100 (d).

specimens. Also, no changes in the FTIR peak positions were observed for the PAT deposited on control or SAM coated specimens when compared to that of PAT in powder form. This further confirmed that the PAT maintains its pristine form after deposited on alloy surfaces.

### 3. SEM characterization

SEM images with magnifications of 70 $\times$  and 3000 $\times$  were captured for all the alloy specimens used in this study (Fig. 4). Figures 4(a)–4(d) show the SEM images of Ctrl-Co—Cr and SAM-Co—Cr. Control-Co—Cr alloy surfaces were flat with few surface defects (pits and scratches). The surface morphology of SAM-Co—Cr was similar to that of control-Co—Cr alloy. Figures 4(e)–4(h) show the SEM images of Ctrl-PAT specimens. When the drug loading is increased from 25 to 100  $\mu\text{g}/\text{cm}^2$ , the corresponding increase in drug concentration on metal surfaces is clearly visible in the SEM images [Figs. 4(e) and 4(g)]. PAT crystals showed needle shaped morphology on the alloy surfaces [Figs. 4(f) and 4(h)]. Figures 4(i) and 4(l) show SEM images of SAM-PAT specimens. These images showed that islands of PAT crystals were formed on SAM coated Co—Cr alloy specimens. High magnification SEM images were also captured for both island [Figs. 4(j) and 4(m)] and nonisland [Figs. 4(k) and 4(n)] areas. Needle shaped PAT crystals were observed on island areas [Figs. 4(j) and 4(m)]. An increase in the density and agglomeration of PAT crystals corresponding to increased drug loading is seen in Figs. 4(i), 4(j), 4(l), and 4(m). The density of PAT crystals on the island areas of SAM-PAT was greater than that of control-Co—Cr alloy. However, PAT crystals were not seen on nonisland areas of SAM-PAT specimens [Figs. 4(k) and 4(n)]. PAT forms regions of crystals as well as molecular coating on Co—Cr alloy surfaces.<sup>24</sup> SEM has been useful in studying the mor-

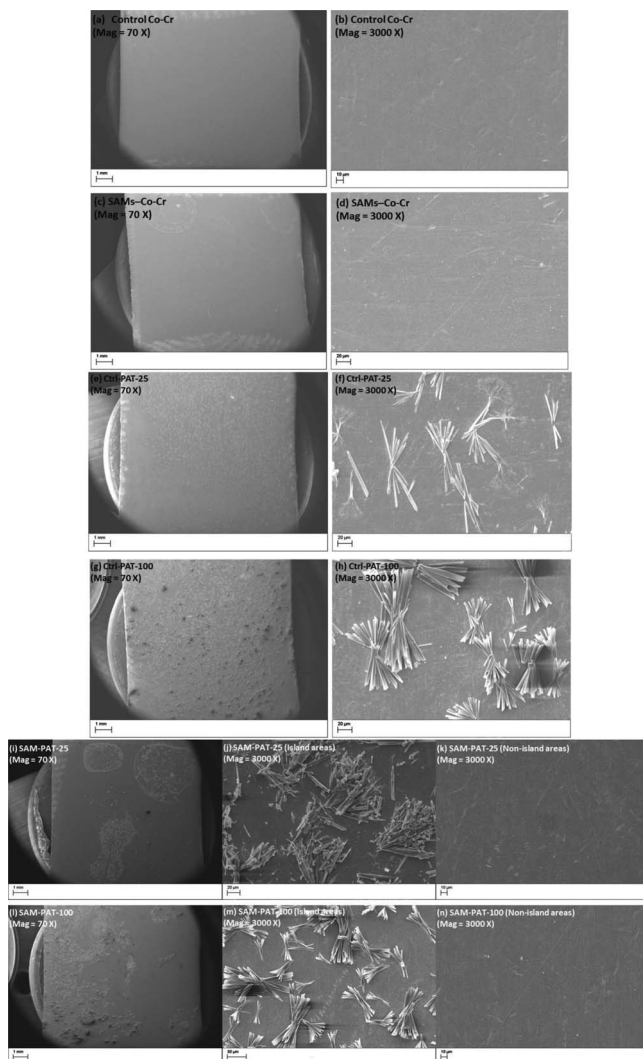


FIG. 4. SEM images of control, SAM coated, and PAT coated specimens.

phology of PAT crystals, while AFM has been useful in studying the molecular coatings of PAT.<sup>24</sup> In this study, the nonisland areas were investigated using AFM for the presence of molecular coatings of PAT.

#### 4. AFM characterization

Figures 5(a)–5(d) show the AFM tapping mode height and phase images of control and SAM coated Co—Cr alloy specimens. The rms roughness values of control and SAM coated specimens were  $22.6 \pm 6.8$  and  $21.2 \pm 5.0$  nm, respectively. No significant differences in the surface morphology or rms roughness values were observed between control and SAM coated specimens. These results suggested that the SAM coated was uniform and it followed the contour of alloy surfaces.<sup>37–39</sup> After the deposition of PAT on Co—Cr alloy, a significant difference in the surface morphology was observed for both Ctrl-PAT and SAM-PAT specimens [Figs. 5(e)–5(l)]. PAT crystals on control specimens were too large to scan using AFM. Hence, the measurements were carried out on the spots where there were no crystals. Powderlike morphology of PAT was observed on those spots [Figs. 5(f)

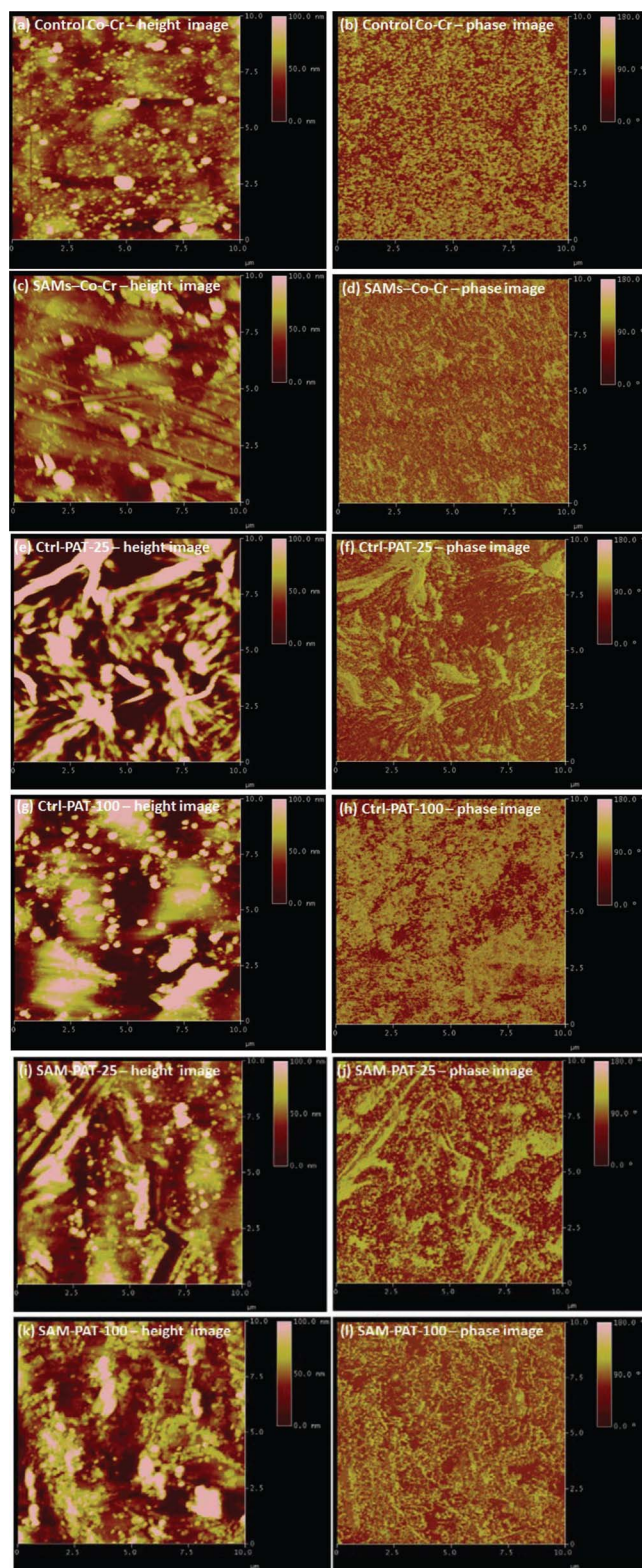


FIG. 5. (Color online) AFM height (a), (c), (e), (g), (i), and (k) and phase (b), (d), (f), (h), (j), and (l) images of control, SAM coated, and PAT deposited specimens.

and 5(h)]. For SAM-PAT specimens, the AFM images were captured only for the nonisland areas. The island areas of PAT crystals were difficult to image due to significant increase in the surface roughness. The nonisland areas of AFM

images showed the distribution of powderlike morphology of PAT [Figs. 5(j) and 5(l)]. These results suggested that when PAT is allowed to deposit on Co—Cr alloy surfaces by the method carried out in this study, it forms needle shaped crystals (as evident from the SEM images) as well as powderlike morphology (as evident from the AFM images).

### B. PAT release from control and SAM coated Co—Cr alloy surfaces

Figures 6(a)–6(d) show the amount of drug released from Ctrl-PAT and SAM-PAT. For Ctrl-PAT-25 [Fig. 6(a)], no significant differences ( $p < 0.05$ ) were observed in the amount of drug released between days 1 and 3 and day 3 and any other time points. However, for SAM-PAT-25 [Fig. 6(b)], significant differences ( $p < 0.05$ ) in the amount of drug released were observed at all initial time points (day 1 and all other time points; day 3 and days 7–35; and day 5 and days 14–35). For Ctrl-PAT-100 [Fig. 6(c)], although there was a significant difference observed between day 1 and days 5–35, no significant differences were observed between other time points including day 3 and days 5–7, day 5 and days 7–21, and day 7 and days 14–35. However, in case of SAM-PAT-100 [Fig. 6(d)], significant differences were observed between several time points including day 1 and days 5–35, day 3 and days 7–35, day 5 and days 14–35, and day 7 and days 21–35.

Figures 6(e)–6(h) show the percentage of total drug release profiles obtained for Ctrl-PAT and SAM-PAT specimens. Burst release profiles were observed for Ctrl-PAT, while biphasic release profiles were observed for SAM-PAT specimens over a period of 35 days. For Ctrl-PAT-25 [Fig. 6(a)], more than 50% of total drug loaded was released within a day. The total drug released by day 3 ( $60\% \pm 3\%$ ) was not significantly different than that of day 35 ( $64\% \pm 3\%$ ). However, in case of SAM-PAT-25 [Fig. 6(b)], only  $21\% \pm 5\%$  of the total drug loaded was released within a day. Also,  $37\% \pm 7\%$ ,  $47\% \pm 7\%$ , and  $53\% \pm 6\%$  of the total drug loaded were released on days 3, 5, and 7, respectively. In Ctrl-PAT-100 [Fig. 6(c)], approximately 50% of the total drug loaded was released within 3 days, while the SAM-PAT-100 showed slow release where percentages of total drug released at 1, 3, 5, 7, 14, 21, 28, and 35 days were  $5\% \pm 2\%$ ,  $10\% \pm 3\%$ ,  $13\% \pm 3\%$ ,  $19\% \pm 3\%$ ,  $23\% \pm 4\%$ ,  $28\% \pm 3\%$ ,  $33\% \pm 5\%$ , and  $40\% \pm 8\%$ , respectively [Fig. 6(d)]. These results suggest that the rate of release of PAT from SAM coated surfaces was slower than that of control surfaces.

### C. SEM characterization of alloy surface postdrug elution

SEM images were also captured for the alloy specimens which were taken out of the PBS/T-20 solution after 35 days of immersion. Figure 7(a) shows the SEM image of Ctrl-PAT-100 after 35 days of PBS/T-20 immersion. No PAT crystals were observed on these specimens which suggested that most of the crystals were released from the specimens in 35 days. Also, these images suggested that the residual drug

retained on the alloy specimens after 35 days of PBS/T-20 immersion might be in the form of molecular coating, which is very difficult to view using a SEM. Figure 7(b) shows the SEM image of SAM-PAT-100 immersed in PBS/T-20 for 35 days. The high density needle shaped residual PAT crystals were observed on these specimens. It is interesting to observe that the PAT crystals were strongly adsorbed on SAM coated Co—Cr alloy surfaces and some of the crystals were not removed even after 35 days of PBS/T-20 immersion. This result demonstrates the high affinity of PAT toward SAM-Co—Cr alloy surfaces.

### D. Discussion

Owing to limitations of polymeric carriers in drug-eluting stents,<sup>11–21</sup> the development of polymer-free drug delivery platforms has potential applications in stents.<sup>10</sup> Surface modification using SAMs is one of the promising techniques for delivering drugs from metal implants without polymeric carriers.<sup>22,23</sup> Our previous studies have shown that a model drug (flufenamic acid) can be released from model substrates (gold and titanium) for a period of 4 weeks using SAMs.<sup>22</sup> The amount of drug coated using SAMs was  $\sim 100$  ng/cm<sup>2</sup>.<sup>22</sup> The drug release showed an initial burst followed by a slow release.<sup>22</sup> Although these studies have shown the potential for using SAMs to deliver drugs from stents, improvements in certain areas are crucial for using this technology in clinical applications. Hence, the objective of this study is to use the SAM technology to deliver an *antiproliferative drug* (paclitaxel) from a *stent material* (Co—Cr alloy) in *clinically relevant doses* ( $\mu\text{g}/\text{cm}^2$ ).

316L stainless steel and Co—Cr alloys are the alloy systems that are commonly used for making coronary stents.<sup>9</sup> Co—Cr alloy is preferred over other metals because of its ability to make ultrathin stent struts with increased strength.<sup>16</sup> Two of the five FDA approved drug-eluting stents are made up of Co—Cr alloy.<sup>9,16</sup> Phosphonic acid SAMs have been successfully coated on 316L stainless steel,<sup>37</sup> titanium,<sup>44</sup> and nitinol.<sup>39</sup> Hence, we expect this SAMs based drug delivery approach to work on several other metal oxide systems as well.

In our previous study, we have used —OH terminated phosphonic acid and thiol SAMs on titanium and gold, respectively.<sup>22</sup> Phosphonic acid SAMs are commonly coated on several metal oxide systems than thiol SAMs.<sup>37,39,44</sup> Hence, we used phosphonic acid SAMs to coat Co—Cr alloy. Also, in our previous study, we have used the model drug flufenamic acid to derivatize —OH terminated SAMs since the drug contains —COOH groups.<sup>22</sup> In the current study, PAT contains —OH groups. Hence, we used —COOH terminated SAMs for PAT derivatization. Although the main interaction expected between PAT and SAMs is the extensive hydrogen bonding, the possibility of esterification reaction between —COOH groups of SAMs and —OH groups of PAT is not ignored. The different bonding interactions between PAT and SAMs are described in detail later in this section.

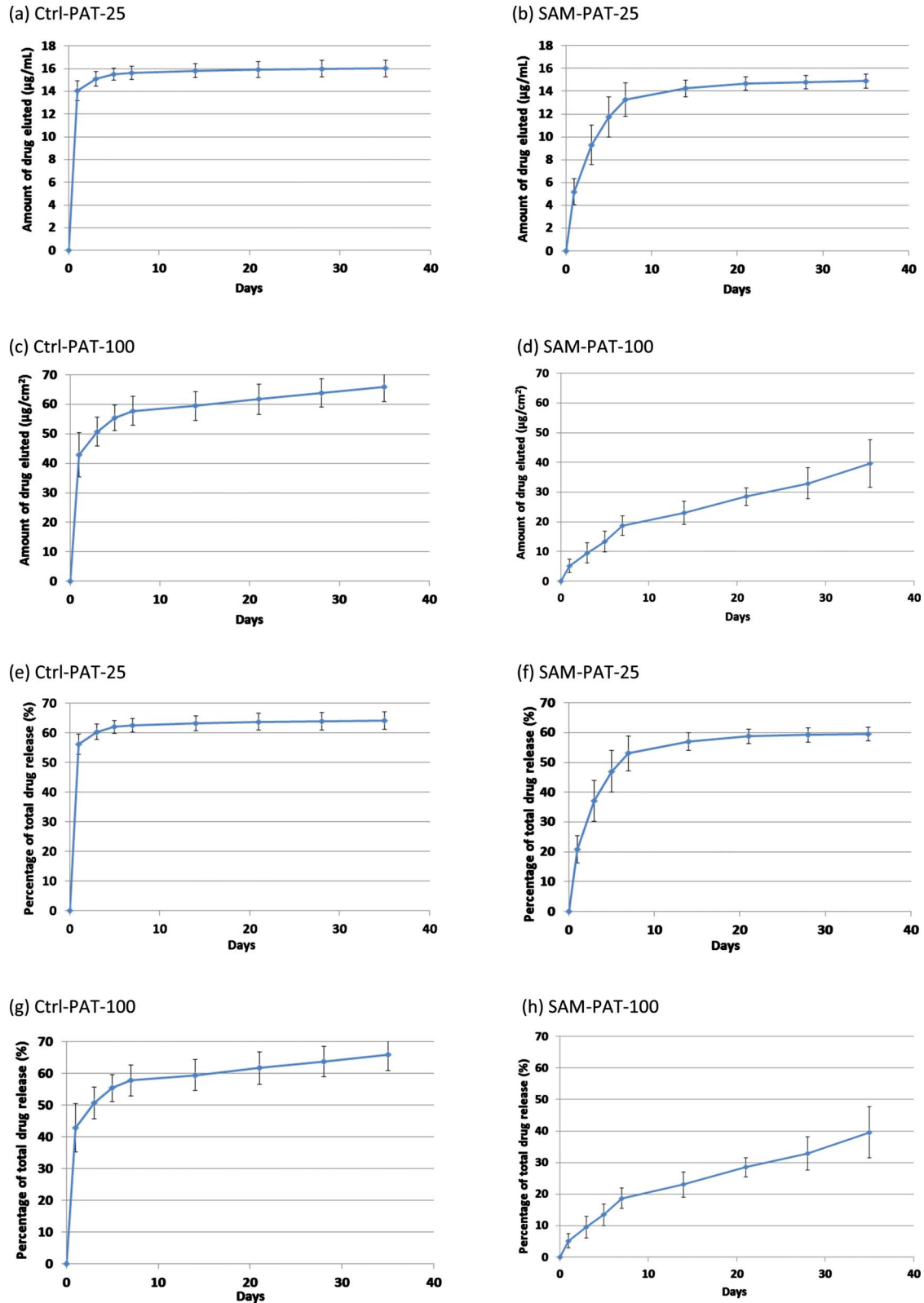


FIG. 6. (Color online) Amount of drug release profiles of Ctrl-PAT-25 (a), SAM-PAT-25 (b), Ctrl-PAT-100 (c), and SAM-PAT-100 (d). Percentage of drug release profiles of Ctrl-PAT-25 (e), SAM-PAT-25 (f), Ctrl-PAT-100 (g), and SAM-PAT-100 (h).

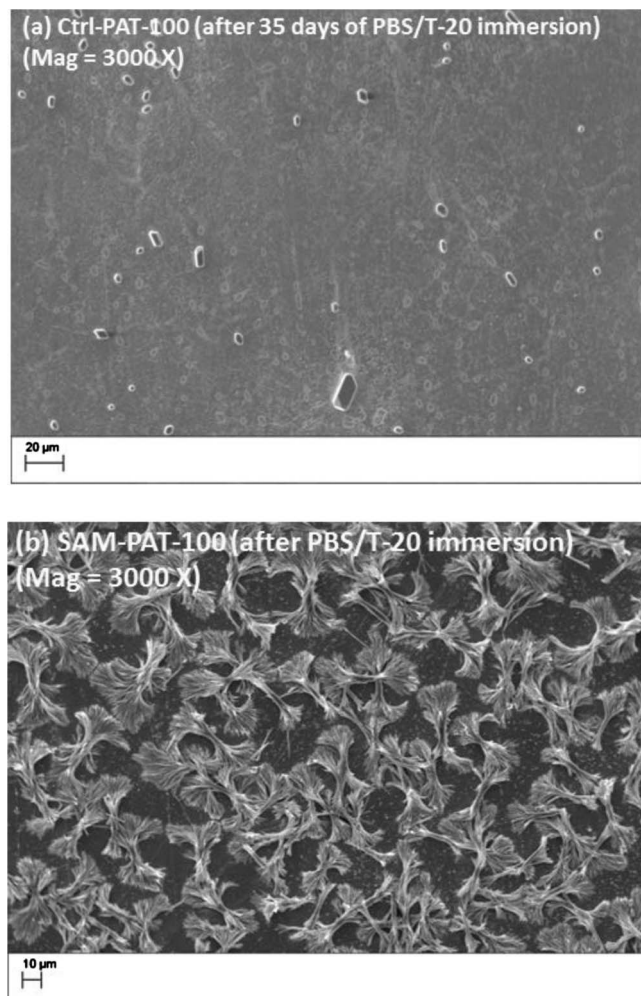


FIG. 7. SEM images of Ctrl-PAT-100 (a) and SAM-PAT-100 (b) after 35 days of PBS/T-20 immersion.

Most commercially available drug-eluting stents typically have a drug loading of  $100 \mu\text{g}/\text{cm}^2$ ,<sup>45</sup> although some stents use lesser amount of drug ( $20 \mu\text{g}/\text{cm}^2$ ).<sup>46</sup> Hence, we have chosen two different drug doses of 25 and  $100 \mu\text{g}/\text{cm}^2$  in this study. Initially, well-ordered and uniform phosphonic acid SAMs were coated on Co—Cr alloy. The two different drug doses of PAT were coated on SAM-Co—Cr alloy surfaces using a microdrop method as previously described.<sup>24</sup> Experiments were also carried out to coat PAT directly on control-Co—Cr alloy specimens (with no SAM coating).

The native surface oxide of Ctrl-Co—Cr alloy is typically enriched with —OH groups.<sup>24</sup> When PAT is deposited on alloy oxides by ethanol evaporation, it forms strongly bound molecular coating as well as weakly bound drug crystals.<sup>24</sup> It was hypothesized that the strongly bound molecular coating occurs between the PAT molecules and high density surface hydroxyl groups of Co—Cr alloy.<sup>24</sup> PAT crystals are formed due to intermolecular hydrogen bonding interactions<sup>47,48</sup> and are present on top of the molecular layer.<sup>24</sup> In this study, SEM images showed the formation of PAT crystals on alloy surfaces and AFM images showed the molecular distribution of PAT in powderlike form. The ions in PBS/T-20 interfere

with hydrogen bonding interactions of PAT crystals<sup>49</sup> and result in the burst release of crystals.<sup>24</sup> This is clearly evident from the burst release profiles observed in this study for Ctrl-PAT specimens [Figs. 6(a) and 6(c)]. Also, no PAT crystals were observed on Ctrl-PAT specimens after 35 days of PBS/T-20 immersion [Fig. 7(a)]. After 35 days, only 65%–70% of the total drug loaded was released from Ctrl-Co—Cr alloy [Figs. 6(e) and 6(g)]. This suggests that some PAT molecules are strongly adsorbed on Co—Cr alloy surfaces and remains stable under physiological conditions for a period investigated in this study.

In case of SAM-PAT specimens, biphasic release profiles were observed [Figs. 6(b), 6(d), 6(f), and 6(h)]. This demonstrates the significant role of SAMs in delivering PAT from Co—Cr alloy surfaces. SAMs used in this study contain —COOH terminal groups. The —COOH groups contain hydroxyl (—OH) functionalities which are hydrogen bond donors and carbonyl (C=O) functionalities which are hydrogen bond acceptors. PAT contains —OH groups as well as C=O functionalities in ester, ketone, and amide groups. The —OH functionalities of SAM molecules can form hydrogen bonds with —OH groups of PAT, —NH groups of PAT, and C=O functionalities of ester, ketone, and amide groups in PAT. Hence, when PAT is allowed to deposit on SAM coated Co—Cr alloy surfaces, the PAT can form extensive hydrogen bonding with SAMs. Also, the heat treatment involved in the drug attachment protocol can facilitate esterification reaction between —COOH groups of SAM and —OH groups of PAT. Carboxylic acid groups can react with hydroxyl groups during dry heating to form covalent ester linkages.<sup>50–52</sup> Thermal esterification (or dry heat esterification) has been commonly reported for —COOH and —OH groups containing systems such as starch/xanthan gum,<sup>50</sup> poly(vinyl alcohol)/poly(acrylic acid),<sup>51</sup> and carboxylic acid-functionalized polyethylene/poly(vinyl alcohol).<sup>52</sup> Hence, covalent ester bonds may also be formed between PAT molecules and SAM. Also, PAT molecules interact with each other through extensive hydrogen bonding.<sup>47</sup> Based on these, we believe that the following three interactions play a vital role in the coating of PAT on SAM coated Co—Cr alloy specimens: (1) hydrogen bonding between PAT molecules and SAMs; (2) covalent bonding (ester bonds) between PAT molecules and SAMs; and (3) intermolecular hydrogen bonding between PAT molecules.

The mechanisms proposed for the PAT delivery from SAMs are as follow: (a) cleavage of hydrogen bonds between PAT molecules and SAMs by the ions in the PBS/T-20 solution; (b) cleavage of ester bonds between PAT and SAM by hydrolysis; and (c) cleavage of hydrogen bonds between PAT molecules by the ions in PBS/T-20 solution. When the density of PAT molecules is high, it provides more stability to drug coating due to extensive intermolecular hydrogen bonding interactions. In the PAT islands of SAM-PAT specimens, the crystals were present in close proximity to each other [Figs. 4(j) and 4(m)]. Hence, there would be more hydrogen bonding between the crystals to make the coating very stable. This could be the reason for the greater stability

of PAT crystals on SAM-Co—Cr specimens resulting in slower release for up to 35 days. However, the PAT crystals were not in close proximity on control-Co—Cr alloy specimens [Figs. 4(f) and 4(h)]. Hence, the hydrogen bonding interactions may not be as great as on SAM coated specimens. This could be the reason for the poor stability of PAT crystals on Ctrl- Co—Cr specimens resulting in burst release.

#### IV. SUMMARY AND CONCLUSIONS

In summary, the —COOH terminated phosphonic acid SAMs were coated on Co—Cr alloy surfaces. A microdrop deposition method was used to load PAT at doses of 25 and 100  $\mu\text{g}/\text{cm}^2$  on SAM coated Co—Cr alloy surfaces. In parallel, control experiments were carried out to deposit PAT on Co—Cr alloy surfaces with no SAM coating. Thus, prepared PAT deposited specimens were characterized using FTIR, SEM, and AFM. FTIR showed that PAT was successfully deposited on SAM coated and control-Co—Cr alloy surfaces. SEM images showed the formation of needle shaped PAT crystals on alloy surfaces. Also, these images showed the islands of high density PAT crystals on SAM coated surfaces, while low density PAT crystals were observed on control surfaces. In addition to crystal deposits, AFM images showed molecular coatings of PAT in powderlike morphology on SAM coated and control-Co—Cr alloy surfaces. *In vitro* drug release studies showed biphasic release profiles (an initial burst release in 7 days was followed by a slow release for up to 35 days) for SAM coated surfaces, while burst release within 3 days was observed for control surfaces. Thus, this study demonstrated the use of SAMs for delivery of antiproliferative drugs from stent material surfaces in doses comparable to those employed in commercially available stents.

#### ACKNOWLEDGMENTS

This work was supported by a National Scientist Development Grant Award (Grant No. 10SDG2630103) from the American Heart Association (AHA). The authors are grateful to the AHA for providing financial support.

- <sup>1</sup>P. Brubaker, M. Whaley, and L. Kaminsky, *Coronary Artery Disease: Essentials of Prevention and Rehab Programs* (Human Kinetics, Champaign, 2001).
- <sup>2</sup>G. Dorros and S. H. Stertz, *Appl. Radiol.* **12**, 69 (1983).
- <sup>3</sup>A. R. Wilson and J. C. Fuchs, *Surg. Clin. North Am.* **64**, 121 (1984).
- <sup>4</sup>P. W. Serruys *et al.*, *N. Engl. J. Med.* **331**, 489 (1994).
- <sup>5</sup>D. L. Fischman *et al.*, *N. Engl. J. Med.* **331**, 496 (1994).
- <sup>6</sup>N. Kipshidze, G. Dangas, M. Tsapenko, J. Moses, M. B. Leon, M. Kutryk, and P. Serruys, *J. Am. Coll. Cardiol.* **44**, 733 (2004).
- <sup>7</sup>A. C. Newby and A. B. Zaltsman, *J. Pathol.* **190**, 300 (2000).
- <sup>8</sup>C. R. Narins and S. G. Ellis, *Semin Interv. Cardiol.* **3**, 91 (1998).
- <sup>9</sup>S. Garg and P. W. Serruys, *J. Am. Coll. Cardiol.* **56**, S1 (2010).
- <sup>10</sup>S. Garg and P. W. Serruys, *J. Am. Coll. Cardiol.* **56**, S43 (2010).
- <sup>11</sup>Y. Otsuka, N. Chronos, R. Apkarian, and K. Robinson, *J. Invasive Cardiol.* **19**, 71 (2007).
- <sup>12</sup>R. Virmani *et al.*, *Circulation* **109**, 701 (2004).

- <sup>13</sup>R. Virmani, F. Kolodgie, and A. Farb, *Am. Heart Hosp. J.* **2**, 85 (2004).
- <sup>14</sup>R. Virmani, A. Farb, G. Guagliumi, and F. Kolodgie, *Coron. Artery Dis.* **15**, 313 (2004).
- <sup>15</sup>J. R. Nebeker *et al.*, *J. Am. Coll. Cardiol.* **47**, 175 (2006).
- <sup>16</sup>G. Mani, M. D. Feldman, D. Patel, and C. M. Agrawal, *Biomaterials* **28**, 1689 (2007).
- <sup>17</sup>E. P. McFadden *et al.*, *Lancet* **364**, 1519 (2004).
- <sup>18</sup>I. Iakovou *et al.*, *JAMA, J. Am. Med. Assoc.* **293**, 2126 (2005).
- <sup>19</sup>A. T. L. Ong, E. P. McFadden, E. Regar, P. P. T. de Jaegere, R. T. van Domburg, and P. W. Serruys, *J. Am. Coll. Cardiol.* **45**, 2088 (2005).
- <sup>20</sup>M. Joner *et al.*, *J. Am. Coll. Cardiol.* **48**, 193 (2006).
- <sup>21</sup>A. V. Finn, G. Nakazawa, M. Joner, F. D. Kolodgie, E. K. Mont, H. K. Gold, and R. Virmani, *Arterioscler., Thromb., Vasc. Biol.* **27**, 1500 (2007).
- <sup>22</sup>G. Mani, D. M. Johnson, D. Marton, M. D. Feldman, D. Patel, A. Ayon, and C. M. Agrawal, *Biomaterials* **29**, 4561 (2008).
- <sup>23</sup>G. Mani, B. Chandrasekar, M. D. Feldman, D. Patel, and C. M. Agrawal, *J. Biomed. Mater. Res., Part B: Appl. Biomater.* **90B**, 789 (2009).
- <sup>24</sup>G. Mani, C. E. Macias, M. D. Feldman, D. Marton, S. Oh, and C. M. Agrawal, *Biomaterials* **31**, 5372 (2010).
- <sup>25</sup>L. Sipos, A. Som, R. Faust, R. Richard, M. Schwarz, S. Ranade, M. Boden, and K. Chan, *Biomacromolecules* **6**, 2570 (2005).
- <sup>26</sup>T. G. Kim, H. Lee, Y. Jang, and T. G. Park, *Biomacromolecules* **10**, 1532 (2009).
- <sup>27</sup>H. J. Lim, H. Y. Nam, B. H. Lee, D. J. Kim, J. Y. Ko, and J. S. Park, *Biotechnol. Prog.* **23**, 693 (2007).
- <sup>28</sup>F. Innocente *et al.*, *Circulation* **120**, S37 (2009).
- <sup>29</sup>D. Song, L. F. Hsu, and J. L. Au, *J. Pharm. Sci.* **85**, 29 (1996).
- <sup>30</sup>J. J. Palmgren, J. Monkonen, T. Korjamo, A. Hassinen, and S. Auriola, *Eur. J. Pharm. Biopharm.* **64**, 369 (2006).
- <sup>31</sup>D. V. Kilpadi, G. N. Raikar, J. Liu, J. E. Lemons, Y. Vohra, and J. C. Gregory, *J. Biomed. Mater. Res.* **40**, 646 (1998).
- <sup>32</sup>N. Adden, L. J. Gamble, D. G. Castner, A. Hoffmann, G. Gross, and H. Menzel, *Langmuir* **22**, 8197 (2006).
- <sup>33</sup>G. Mani, M. D. Feldman, S. Oh, and C. M. Agrawal, *Appl. Surf. Sci.* **255**, 5961 (2009).
- <sup>34</sup>A. Nanci, J. D. Wuest, L. Peru, P. Brunet, V. Sharma, S. Zalzal, and M. D. McKee, *J. Biomed. Mater. Res.* **40**, 324 (1998).
- <sup>35</sup>G. Mani, D. Johnson, D. Marton, V. L. Dougherty, M. D. Feldman, D. Patel, A. Ayon, and C. M. Agrawal, *Langmuir* **24**, 6774 (2008).
- <sup>36</sup>C. R. Kaufmann, G. Mani, D. Marton, D. M. Johnson, and C. M. Agrawal, *Biomed. Mater.* **5**, 025008 (2010).
- <sup>37</sup>A. Raman, M. Dubey, I. Gouzman, and E. S. Gawalt, *Langmuir* **22**, 6469 (2006).
- <sup>38</sup>A. Raman and E. S. Gawalt, *Langmuir* **23**, 2284 (2007).
- <sup>39</sup>R. Quiñones and E. S. Gawalt, *Langmuir* **23**, 10123 (2007).
- <sup>40</sup>A. Raman, R. Quinones, L. Barriger, R. Eastman, A. Parsi, and E. S. Gawalt, *Langmuir* **26**, 1747 (2010).
- <sup>41</sup>E. Suleymanoglu, *Electron J Biomed.* **3**, 19 (2009).
- <sup>42</sup>A. B. Dhanikula and R. Panchagnula, *Curr. Drug Deliv.* **2**, 75 (2005).
- <sup>43</sup>R. T. Liggins, W. L. Hunter, and H. M. Burt, *J. Pharm. Sci.* **86**, 1458 (1997).
- <sup>44</sup>E. S. Gawalt, M. J. Avaltroni, N. Koch, and J. Schwartz, *Langmuir* **17**, 5736 (2001).
- <sup>45</sup>K. Kamath, J. J. Barry, and K. M. Miller, *Adv. Drug Delivery Rev.* **58**, 412 (2006).
- <sup>46</sup>A. König, M. Leibig, J. Rieber, T. M. Schiele, K. Theisen, U. Siebert, R. M. Gothe, and V. Klauss, *Am. Heart J.* **153**, 979 (2007).
- <sup>47</sup>D. Mastropaolo, A. Camerman, Y. Luo, G. D. Brayer, and N. Camerman, *Proc. Natl. Acad. Sci. U.S.A.* **92**, 6920 (1995).
- <sup>48</sup>I. H. Lee, Y. T. Park, K. Roh, H. Chung, I. C. Kwon, and S. Y. Jeong, *J. Controlled Release* **102**, 415 (2005).
- <sup>49</sup>S. Kim, J. Y. Kim, K. M. Huh, G. Acharya, and K. Park, *J. Controlled Release* **132**, 222 (2008).
- <sup>50</sup>H. S. Lim, J. N. BeMiller, and S. T. Lim, *Cereal Chem.* **80**, 198 (2003).
- <sup>51</sup>K. Kumeta, I. Nagashima, S. Matsui, and K. Mizoguchi, *J. Appl. Polym. Sci.* **90**, 2420 (2003).
- <sup>52</sup>R. Silva, E. C. Muniz, and A. F. Rubira, *Polymer* **49**, 4066 (2008).